Clays and Clay Minerals, Vol. 50, No. 2, 223–239, 2002.

SITE OCCUPANCIES BY IRON IN NONTRONITES

W. P. GATES[1,*], P. G. SLADE[1], A. MANCEAU[2] AND B. LANSON[2]

[1] CSIRO Land and Water, PMB No 2, Glen Osmond, SA 5064 Australia
[2] Environmental Geochemistry Group, LGIT-IRIGM, University Joseph Fourier and CNRS, BP 53, 38041 Grenoble Cedex 9, France

Abstract—Twelve nontronites and two ferruginous smectites have been characterized with respect to Fe^{3+} occupancy of tetrahedral sites. The techniques used were near infrared, Fe-K X-ray absorption near-edge and X-ray absorption fine-structure spectroscopies, along with two X-ray diffraction techniques. The results show that calculations of the structural formulae of many nontronites should be adjusted to include Fe^{3+} in tetrahedral sites. The nontronite from Spokane County, Washington, (~44% Fe_2O_3) is essentially an end-member with its non-siliceous tetrahedral sites occupied by Fe^{3+}. Samples with chemical compositions similar to Garfield nontronite (~36.5% Fe_2O_3) may have small amounts (<5% of total Fe^{3+}) of tetrahedral Fe^{3+}. Tetrahedral Fe^{3+} is unlikely to be present in samples containing less than ~34% Fe_2O_3.

Key Words—Chemical Analyses, EXAFS, Near IR, Nontronites, Octahedral Fe, Site Occupancy, Smectites, Structural Formula, Tetrahedral Fe, XANES, X-ray Diffraction

INTRODUCTION

In order to calculate the structural formulae of minerals, their analytically-determined cations must be correctly distributed over the available structural sites. However, a particular difficulty arises for the layer silicates as Fe^{3+} and Al can each occupy both octahedral and tetrahedral cation sites. Aluminum is assigned to the non-siliceous tetrahedral sites in preference to Fe^{3+}, but when insufficient Al is available to fill these tetrahedral sites, Fe^{3+} is directed to them. Mössbauer spectroscopic evidence shows that the conventional filling of the tetrahedral sites with Al, prior to assigning Fe^{3+}, in trioctahedral micas (Dyar, 1987, 1993; Rancourt *et al*., 1992; Rancourt, 1993) and some vermiculites (Cardile and Slade, 1988) may be incorrect. By using infrared (IR) spectroscopy, Besson *et al*. (1987) demonstrated that the conventional calculation of the structural formulae of dioctahedral micaceous minerals (glauconites and celadonites) may be incorrect. For Al-poor and Fe-rich 2:1 layer silicates, such as nontronites (Eggleton, 1977), the conventional method for calculating structural formulae may especially be invalid, and thus spectroscopic or other techniques are needed to correctly determine the Al and Fe^{3+} site occupancies.

Spectroscopic methods which have been employed to determine site occupancies in nontronites include Mössbauer (Goodman *et al*., 1976; Besson *et al*., 1983; Bonnin *et al*., 1985; Cardile and Johnston, 1985; Sherman and Vergo, 1988; Luca and Cardile, 1989; Murad, 1987; Luca, 1991), IR (Goodman *et al*., 1976; Madejová *et al*., 1994; Bishop *et al*., 1999), optical (Sherman and Vergo, 1988; Bishop *et al*., 1999) and X-ray absorption spectroscopies (XAS) (Bonnin *et al*., 1985; Manceau *et al*., 1990, 1998, 2000). Diffraction methods have also been employed for site occupancy determinations (Besson *et al*., 1983; Manceau *et al*., 1998, 2000). Measurements of magnetic ordering have been used by Lear and Stucki (1990) and by Murad *et al*. (1990) to support assignments. For the standard Garfield nontronite from Whitman Co., Washington, the application of these methods has led to disagreement in assigning Fe^{3+} to tetrahedral sites (Goodman *et al*., 1976; Besson *et al*., 1983; Bonnin *et al*., 1985; Cardile and Johnston, 1985; Murad, 1987; Sherman and Vergo, 1988; Luca, 1991; Manceau *et al*., 2000). That these spectroscopic techniques have been only partially successful, is due in part to confusion over the exact identities and localities of some samples (*e.g.* Garfield (API H33a), Manito (API H33b) and Spokane) and to inaccurate chemical analyses due to impurities. Problems in spectral interpretation may occur when the chemical analyses relied upon do not apply to the exact portion of the material that is measured spectroscopically.

The present paper reports the combined use of near infrared (NIR), X-ray pre-edge and extended X-ray absorption fine-structure (EXAFS) spectroscopies, and also of X-ray diffraction (XRD) to determine the distributions of Fe in a series of 12 carefully purified and chemically analyzed nontronites and two ferruginous smectites. The results are compared with those given in other studies.

MATERIALS AND METHODS

Purification and chemical analysis

The identifications of the nontronites and ferruginous smectites used, along with their source localities and chemical analyses are given in Table 1. No previous results for these samples were taken at face value, and so all samples were carefully purified for this work by

* E-mail address of corresponding author:
will.gates@adl.clw.csiro.au

Table 1. Samples studied and their chemical analyses (ignited basis) as determined by XRF.

Sample‡	SiO_2	TiO_2	Al_2O_3	Fe_2O_3	MnO	MgO	CaO	Na_2O	K_2O	P_2O_5	SO_3	ZrO_2	Sr	Sum
							%†							
(1) Fe-smectite W. Australia	59.31	0.052	12.72	21.52	0.002	2.061	2.497	0.097	1.477	0.004	0.005	0.002	0.000	99.75
(2) SWa-1, Washington	56.68	0.540	11.04	26.65	0.014	1.302	3.164	0.254	0.007	0.025	0.000	0.016	0.002	99.69
(3) Cheney, Washington	52.93	1.282	12.37	29.39	0.013	0.269	3.375	0.110	0.018	0.038	0.000	0.008	0.002	99.76
(4) Giralong, New South Wales	54.97	0.038	6.853	33.39	0.040	1.411	3.089	0.163	0.012	0.005	0.004	0.001	0.002	99.98
(5) Manito, Washington	52.23	0.114	7.717	35.21	0.023	0.603	3.462	0.048	0.026	0.023	0.021	0.005	0.001	99.49
(6) NAu-1, South Australia	51.36	0.201	8.150	35.94	0.013	0.191	3.565	0.033	0.006	0.011	0.001	0.004	0.001	99.48
(7) Bingham, Utah	52.70	0.247	5.530	36.28	0.010	1.128	3.449	0.134	0.082	0.002	0.006	0.004	0.000	99.57
(8) Garfield, Washington	51.68	0.000	7.546	36.43	0.014	0.158	3.524	0.183	0.016	0.029	0.003	0.001	0.001	99.66
(9) Mountainville, Pennsylvania	51.87	0.000	7.411	36.98	0.007	0.207	3.505	0.095	0.000	0.000	0.000	0.087	0.053	100.3
(10) NG-1, Germany	52.30	0.000	6.056	37.50	0.002	0.258	3.226	0.026	0.033	0.007	0.006	0.000	0.000	99.41
(11) NAu-2, South Australia	56.18	0.020	3.114	37.85	0.016	0.255	2.342	0.143	0.013	0.001	0.004	0.014	0.003	99.92
(12) HQ, Tasmania	51.34	0.026	6.871	38.04	0.000	0.153	3.540	0.000	0.009	0.021	0.000	0.000	0.000	100.0
(13) Spokane, Washington	52.29	0.000	0.413	43.88	0.007	0.169	3.018	0.078	0.000	0.002	0.000	0.000	0.000	99.85
(14) CZ, Germany	50.31	0.000	1.655	44.23	0.000	0.168	3.308	0.011	0.008	0.014	0.009	0.000	0.000	99.71

† estimated errors are: Si 0.1%; Ti 0.01%

‡ (1) from I. Pontifex; (2), (10), Source Clays Repository, The Clay Minerals Society; (3), (5), (7), (8) Ward's Natural Science Establishment; (4) T. Eggleton, Australian National Museum; (6), (11) collected by first author, now available from the Source Clays Repository (Keeling *et al*., 2000); (9) Excalibur minerals; (12), (13) CSIRO Land and Water Mineral Collection; (14) S. Hillier, Macaulay Land Use Research Institute

saturating them initially with either Na^+ or Li^+ and then washing them by centrifugation to obtain dispersed fine fractions. These were checked by XRD using random and oriented powder methods. The pure fine fractions were Ca saturated and dialyzed to remove excess salts. Depending on the sample, the fractions were composed of either < 0.5, <0.2, < 0.15 or <0.1 μm particles. For sample NAu-2, an overnight treatment of the <0.1 μm fraction with 0.1 M Na acetate was needed to remove carbonates. All materials were finally oven dried at 105°C. The nontronites NAu-1, Garfield (8), NG-1 (10), NAu-2 (11) and Spokane (13) were free of Fe oxide phases, as was tested with low-temperature Mössbauer spectroscopy. The recently discovered nontronites NAu-1 and NAu-2 (Keeling *et al*., 2000) were checked by transmission electron microscopy (TEM) with energy dispersive analysis. Chemical analyses using X-ray fluorescence (XRF) spectroscopy, following the procedures of Norrish and Hutton (1969), were performed on the purified, Ca-saturated, ignited (1050°C) samples. Conventional structural formulae, based on 22 oxygen equivalents, were calculated from these analyses with the program CLAYFORM (Bodine, 1987) and are shown in Table 2. The chemical analysis of Fe smectite from West Australia showed a relatively high K_2O value (sample 1, Table 1), and therefore it may contain interstratified illite, which potentially could lower the octahedral Al content given in the calculated structural formula (Table 2).

Near infrared spectroscopy

Diffuse reflectance spectra (512 scans at 2 cm^{-1} resolution) in the NIR region were collected on a Biorad FTS 175C Fourier transform spectrophotometer fitted with a CsI beamsplitter and a solid-state (DTGS) detector. Samples were front packed into the sample cell to present random powders and spectra were referenced to KBr powder.

The NIR region was used to determine octahedral occupancies from combination bands because the characteristic hydroxyl vibrations associated with octahedral cations, which occur in the mid infrared (MIR) region, are often masked by overlapping bands. For example, AlAlOH-bending bands near 912 cm^{-1} are shoulders on the Si–O-stretching band (1020 cm^{-1}) in the MIR. Likewise, the AlFeOH-stretching vibrations

Table 2. Structural formulae of nontronites and ferruginous smectites as calculated conventionally by CLAYFORM (22 oxygen equivalents).

	1	2	3	4	5	6	7	8	9	10	11	12	13	14
Tetrahedral														
Si	7.58	7.40	7.06	7.32	7.07	6.98	7.17	7.02	7.01	7.12	7.55	6.98	7.26	7.04
Al	0.42	0.60	0.94	0.68	0.93	1.02	0.83	0.98	0.99	0.88	0.45	1.02	0.07	0.27
Fe													0.67	0.69
Σ	8.00	8.00	8.00	8.00	8.00	8.00	8.00	8.00	8.00	8.000	8.00	8.00	8.00	8.00
Octahedral														
Al	1.49	1.10	1.00	0.39	0.30	0.29	0.06	0.23	0.19	0.10	0.05	0.08		
Fe	2.07	2.62	2.95	3.34	3.59	3.68	3.71	3.72	3.76	3.84	3.83	3.89	3.92	3.96
Mg	0.39	0.25	0.05	0.28	0.12	0.04	0.23	0.03	0.04	0.05	0.05	0.03	0.03	0.04
Σ	3.95	3.97	4.00	4.01	4.01	4.00	4.00	3.98	3.99	3.99	3.93	4.00	3.95	4.02
Total Layer Charge														
Tet	0.42	0.60	0.94	0.68	0.93	1.02	0.83	0.98	0.99	0.88	0.45	1.02	0.74	0.96
Oct	0.53	0.35	0.05	0.24	0.09	0.03	0.23	0.09	0.05	0.08	0.27	0.01	0.18	0.03
Σ	0.95	0.95	1.00	0.92	1.02	1.05	1.06	1.07	1.04	0.96	0.72	1.03	0.92	1.00

near 3600 cm^{-1} are hidden within the entire OH-stretching band for nontronites (Madejová *et al*., 1994).

To estimate tetrahedral Fe^{3+} occupancies, the areas for octahedral Al and Fe^{3+} combination bands were fitted, using least-squares, to Lorentzian-Gaussian envelopes, in the ratio of 1:4. The peak positions, intensities and full widths at half-height were varied, without constraint, along with a quadratic baseline. The individual band areas assigned to the AlAlOH and AlFeOH vibrations associated with octahedral Al were then expressed as percentages of the total spectral area between 4700 and 4200 cm^{-1}. An integrated area, comprising 2 × (area associated with AlAlOH) + 1 × (area associated with AlFeOH) was then plotted against the octahedral Al occupancies obtained from the conventionally-calculated structural formulae. A polynomial regression equation was next used to obtain the corrected octahedral Al occupancies from their NIR band areas. The octahedral Al occupancies for samples not showing this relationship were adjusted, using this regression, to improve their fit. Subtraction of the adjusted octahedral Al occupancy values from the total number of Al cations in the unit-cells provided corrected tetrahedral Al occupancies which, on subtraction from the number of non-siliceous sites, enabled an estimate of tetrahedral Fe^{3+} occupancy for each sample to be obtained.

X-ray diffraction

These methods rely on changes to the intensities of X-ray reflections of clay minerals as the relative scattering power of planes containing tetrahedral and octahedral cations change. Iron, as a heavy scatterer compared with Al or Si, has a large effect on this relationship.

X-ray diffraction of non-oriented powders. Diffraction patterns of randomly-oriented, similarly dehydrated, Na-nontronites (samples 2, 6, 8, 10, 11 and 13) were recorded, either in vacuum (10^{-5} T) or at low relative humidity (5% rh, 50°C), with a Siemens D5000 diffractometer using CuKα radiation and equipped with a Kevex Si(Li) solid-state detector. Intensity data were obtained by counting for 40–50 s at intervals of 0.04°2θ. The high vacuum or low rh ensured the complete collapse of the *d*(001) value to 9.6 Å.

Simulated intensity profiles of the 02-11 and 20-13 diffraction bands, over the range 16 to 40°2θ, were calculated using the mathematics given by Plançon (1981), Sakharov *et al*. (1982a,b) and Drits and Tchoubar (1990). Structure factors were calculated from atomic coordinates given by Smoliar-Zviagina (1993). The unit-cell parameters were experimentally determined and entirely *trans*-vacant octahedra were assumed (Manceau *et al*., 2000). The 02-11 and 20-13 reflection intensities were calculated initially using the tetrahedral and octahedral occupancies obtained from the conventional structural formulae (except for sample 13, in which all the non-siliceous tetrahedral sites were occupied by Fe^{3+}). The 02-11 and 20-13 reflection profiles were then refined by adjusting the relative proportions of coherent scattering domains, having radii of either 100 or 200 Å. Finally, the simulated intensities of the 02-11 and 20-13 reflections were fitted to the experimental values by adjusting the tetrahedral Fe^{3+} occupancies.

X-ray diffraction of oriented films. Thin films (20 × 10 mm, ~30 μm thick) were prepared by passing dilute nontronite suspensions through ⩽0.05 μm cellulose acetate filters. The intensities of the 002 and 003 reflections from two stacked self-supporting films of Ca-saturated and ethylene glycol-solvated nontronite, on silicon wafers, were recorded using a Philips PW1710 diffractometer (CoKα radiation), fitted with a 0.5° divergence slit, two Soller slits, graphite monochromator and a proportional counter. Prior to the collection of

intensity data, the basal spacing, $d(001)$, for each sample was confirmed to be within the range 16.8–17.0 Å. Counting was carried out for 3 s at 0.02° intervals between 8 and 21°2θ. Within this angular range, the X-ray beam fell entirely within the sample area, and so a correction was not required for energy loss from the beam. Integrated peak areas above background were used to calculate observed structure amplitudes (F^{obs}_{00l}) for the 002 and 003 reflections using the expression:

$$|F^{obs}_{00l}| \supset \sqrt{\frac{I_{00l}}{Lp_{00l}}} \quad (1)$$

where $I_{(00l)}$ is the integrated peak area,

$Lp_{(00l)} = (1 + \cos^2 2\alpha\cos^2 2\theta)/(1 + \cos^2 2\alpha)(\sin 2\theta \sin \theta)$ is the Lorentz polarization correction when using a monochromator for finely powdered flat specimens, 2θ is the angle of the 00*l* reflection and 2α refers to the diffraction angle (30.99°) of the graphite monochromator used (Klug and Alexander, 1974). For ethylene glycol-solvated, Ca^{2+}-saturated nontronites, 002 occurs at ~12.08° and 003 at ~18.16°2θ for CoKα radiation (1.7902 Å), for which the Lorentz-polarization corrections are 154.7 and 67.6, respectively. The experimentally-derived ratios ($|F|^{obs}_{002}/|F^{obs}_{003}|$) of the 002 and 003 structure amplitudes for the specimens were compared to the ratios obtained from the structure amplitudes calculated for their 002 and 003 reflections using the program ORFLS (Busing *et al.*, 1962). The atomic coordinates of Ca^{2+}-vermiculite (Slade *et al.*, 1985) formed the basis for these calculations, but the *z* coordinates were modified to correspond with Ca^{2+}-saturated, ethylene glycol-solvated specimens (MacEwan and Wilson, 1980). The site occupancy factors for each nontronite sample were obtained from its specific chemistry. Fully ionized atomic scattering factors were used and the temperature factors applied were those given in Slade *et al.* (1985).

X-ray absorption spectroscopy

For Na^+-exchanged samples of SWa-1 (2), NAu-1 (6), Garfield (8), NG-1 (10), NAu-2 (11) and Spokane (13) nontronite, transmission Fe-K X-ray pre-edge and EXAFS spectra were collected on station D42 at LURE (Orsay, France). Nontronite powders were mixed with boron nitride and packed into 0.5 mm thick sample holders with kapton tape windows to provide an absorption jump ($\Delta\mu$ of ~0.5–1.0. Mixed gas (air/helium) ionization chambers were adjusted to attenuate the beam intensity by ~20% before and ~80% after the sample. The spectra were measured at the magic angle to eliminate texture effects (Manceau *et al.*, 1990).

Pre-edge spectra. Pre-edge spectra, acquired near the Fe-K edge, are sensitive to the electronic environment around the Fe atoms. The intensity and shape of pre-edge spectra are dependent on the symmetry of electronic states within the atom, and thus indicate coordination environments of cations in phyllosilicates (Manceau and Gates, 1997; Manceau *et al.*, 2000). Since point group selection rules do not allow 3d transitions, no pre-edge spectral detail should be observed for Fe^{3+} in ideal octahedral environments. However, in minerals, the octahedral Fe^{3+} coordination environments are frequently distorted, and thus, pre-edge spectral lines can exist. These pre-edge energy states of Fe are often split into two t_{2g}- and e_g-like levels separated by ~2 eV, giving rise to a doublet. In contrast, for ideal tetrahedral environments, closely spaced $1s(a_1) \rightarrow t_2$ transitions of Fe^{3+} are allowed, and give rise to a single broad pre-edge spectral line. In addition, for many Fe-containing minerals, the observed amplitude of pre-edge spectra for Fe^{3+} in tetrahedral environments can be as much as 6 to 10 times greater than that of Fe^{3+} in octahedral coordination.

The amounts of tetrahedral Fe^{3+} in unknown samples were calculated by least-squares minimization of differences between the experimental pre-edge spectra and combinations of tetrahedral and octahedral Fe^{3+} reference spectra. Reference and experimental pre-edge spectra were normalized to the main absorption jump following the procedure described in Manceau and Gates (1997). For tetrahedral Fe^{3+}, the reference material was $FePO_4$ synthesized by dehydration of $FePO_4{\cdot}2H_2O$ at 930°C following the method of Remy and Boulle (1961). Its purity was checked by XRD. For octahedral Fe^{3+}, the reference materials used were goethite, hematite and Garfield nontronite. The last was suitable for use as an octahedral Fe^{3+} reference, as its pre-edge spectra has a line shape and intensity suitable for modelling other nontronites. In addition, its tetrahedral Fe^{3+} content is below the detection limits of the method (Manceau and Gates, 1997).

EXAFS spectra. An in-depth discussion on the application of EXAFS to Fe^{3+}-containing clay minerals can be found in Manceau *et al.* (1998, 2000). Analysis of the Fe-K-edge EXAFS spectra provides structural information about coordination environments, interatomic distances, nearest neighbor atoms and oxidation states. Here the first-shell Fe^{3+}–O contributions were specifically examined using the structural information derived from Manceau *et al.* (1998, 2000). Isolation of Fe^{3+}–O contributions to the EXAFS signal allows the average Fe^{3+}–O bond length (R) and the distributions of bond lengths (ΔR) about the average to be determined. The coordination number (N) can then be determined. For Garfield nontronite, Manceau *et al.* (2000) determined N for Fe^{3+} in octahedral sites to be between 5.3 and 6.3.

The EXAFS spectra were extracted from raw X-ray absorption spectra by subtracting the atomic absorption contributions and normalizing the amplitude to the absorption jump ($\Delta\mu$). Radial structure functions (RSF),

Table 3. Amount of tetrahedral Fe^{3+}, per 22 oxygen equivalents ($/O_{20}(OH)_4$), for nontronites and ferruginous smectites. The results were obtained by NIR, X-ray pre-edge and EXAFS spectroscopies, and XRD.

Sample	NIR*		X-ray pre-edge#		EXAFS$		F_{002}/F_{003}&		*hk* profiles!	
	($/O_{20}(OH_4)$)	% of total Fe^{3+}	($/O_{20}(OH_4)$)	% of total Fe^{3+}	($/O_{20}(OH_4)$)	% of total Fe^{3+}	($/O_{20}(OH_4)$)	% of total Fe^{3+}	($/O_{20}(OH_4)$)	% of total Fe^{3+}
1. Fe-smectite	0	0	n.d.		n.d.		n.d.		n.d.	
2. SWa-1	0	0	0	0	0	0	0	0	0	0
3. Cheney	0	0	n.d.		n.d.		0	0	n.d.	
4. Giralong	0	0	n.d.		n.d.		0.10 ± 0.03	0	n.d.	
5. Manito	0	0	n.d.		n.d.		0.23 ± 0.07	3.5–8.5	n.d.	
6. NAu-1	0	0	0	0	0	0	0.26 ± 0.08	4.5–9.5	0	0
7. Bingham	0.13 ± 0.04	2.0–5.0	n.d.		n.d.		0.35 ± 0.08	6.0–11.0	n.d.	
8. Garfield	0	0	0	0	$\leqslant 0.11$	0–3.0	0.30 ± 0.09	5.5–10.5	0	0
9. Mountainville	0.09 ± 0.04	–4.0	n.d.		n.d.		0.34 ± 0.09	6.5–11.5	n.d.	
10. NG-1	0.68 ± 0.05	14.5–19.5	0.46 ± 0.19	8.0–18.0	0.65 ± 0.11	12.0–18.0	0.52 ± 0.09	11.0–16.0	0.63 ± 0.3	0–18.0
11. NAu-2	0.24 ± 0.05	4.5–7.5	0.27 ± 0.19	3.0–13.0	0.31 ± 0.11	5.0–11.0	0.39 ± 0.09	7.5–12.5	0.22 ± 0.2	0–12.0
12. HQ Tasmania	0.42 ± 0.05	9.5–12.5	n.d.		n.d.		0.41 ± 0.10	8.5–13.5	n.d.	
13. Spokane	0.74 ± 0.06	14.5–17.5	0.46 ± 0.23	7.0–17.0	0.57 ± 0.14	9.0–15.0	0.74 ± 0.11	13.5–18.5	0.74 ± 0.3	0–16.0
14. CZ Germany	0.91 ± 0.07	18.5–21.5	n.d.		n.d.		0.92 ± 0.12	17.5–22.5	n.d.	

* based on non-linear regression of normalized integrated intensities of NIR spectra, error estimated as $\pm 1.5\%$ of total Fe^{3+}.
# based on simulated X-ray pre-edge spectra, error estimated as $\pm 5\%$ of total Fe^{3+} (Manceau and Gates, 1997).
$ based on simulations of Fe–O bond distance and coordination numbers, error estimated as $\pm 3\%$ of total Fe^{3+} (Manceau *et al.*, 2000).
& based on comparisons of calculated (sample dependent) and observed F_{002}/F_{003} ratios, error estimated as $\pm 2.5\%$ of total Fe^{3+}.
! based on simulations of *hk* profiles, error estimated as $\pm 50\%$ of non-siliceous tetrahedral sites.
n.d. = not determined

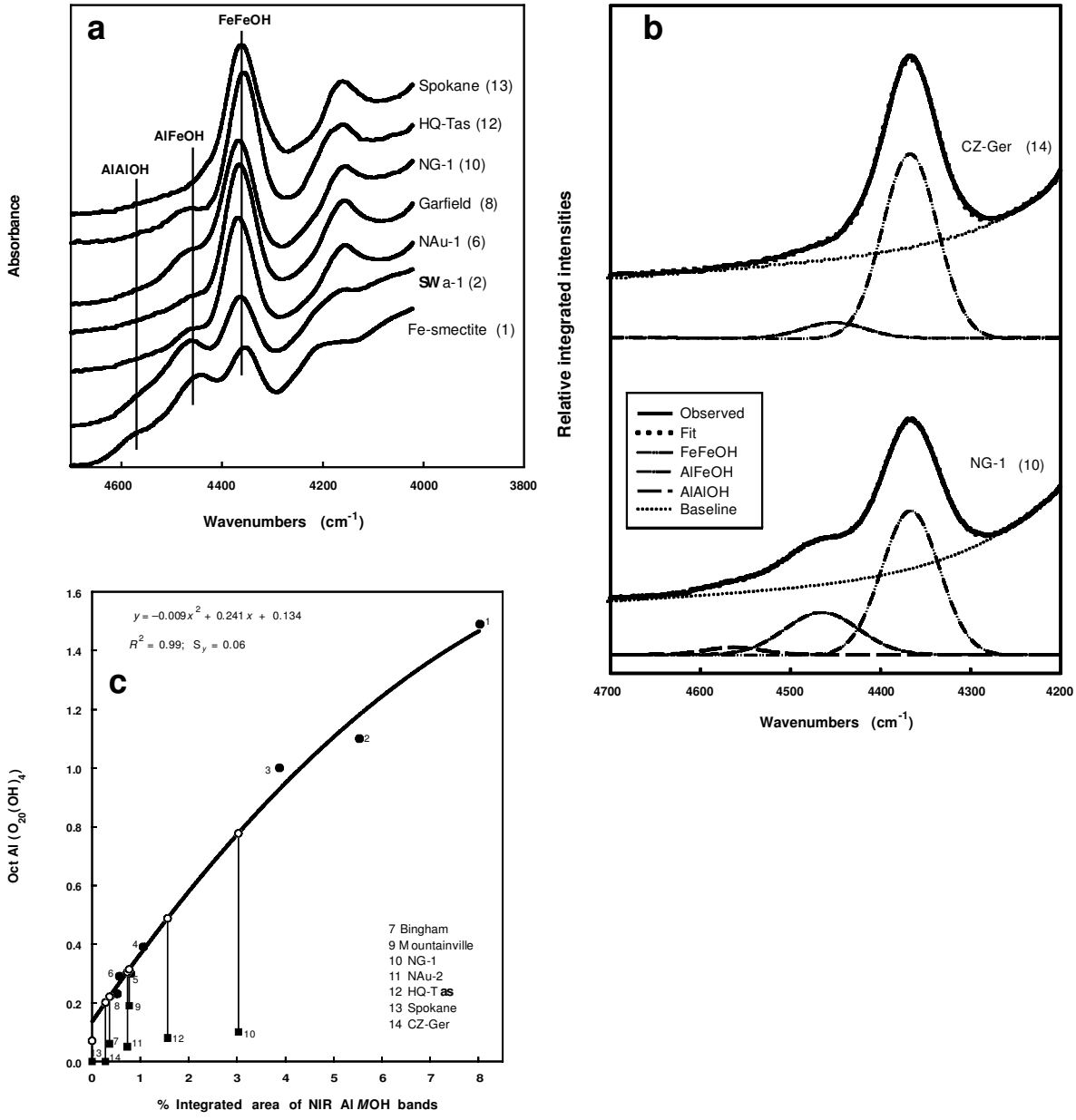

Figure 1. (a) The octahedral *MM*OH (where *M* = Al, Fe) combination bands within the NIR region. (b) Decomposition of the Al*M*OH bands of NG-1 (10) and CZ-Ger (14) nontronites. (c) Predictive relationship between the integrated areas of the NIR Al*M*OH bands and octahedral Al content per unit-cell of nontronites and ferruginous smectites. Vertical lines connect data (filled squares), in which NIR indicates samples to have significantly more octahedral Al than conventional assignments would suggest, to the corrected values (open circles) after applying the polynomial regression (best fit of filled circles).

uncorrected for phase shift, were obtained by Fourier transformation of the EXAFS spectra. The first oxygen shell of the RSF for each sample was further analyzed by Fourier back-transformation to produce waveforms depicting the Fe–O contributions to the EXAFS signal. These experimental Fe–O waveforms were then compared to linear combinations of calculated waveforms for 4-fold and 6-fold coordinated Fe^{3+}, using average Fe–O bond distances of 1.85 and 2.02 Å, respectively. The tetrahedral Fe^{3+} contents of the nontronite samples were obtained by least-squares fitting to the calculated waveforms.

RESULTS AND DISCUSSION

Table 2 shows that the conventional assignments of Al and Fe^{3+} to tetrahedral and octahedral sites would only place Fe^{3+} in the tetrahedral sites of the Spokane (13) and Clausthal Zellerfeld (CZ-Ger; 14) nontronites.

These two samples have very low Al contents, <1.7% Al_2O_3, and thus are essentially nontronite end-members.

Results from the various methods used here are given in Table 3, which shows the tetrahedral Fe^{3+} contents of the samples per 22 oxygen equivalents, and also as a percentage of their total Fe^{3+} contents. A discussion of the results given by each method follows.

Near infrared region

Figure 1a, shows that the AlAlOH (4572 cm^{-1}) and AlFeOH (4470 cm^{-1}) combination bands become more evident with increasing Al content, illustrating the sensitivity of NIR to the type and distribution of cations in the octahedral sites. Figure 1a also shows that the positions of NIR peaks tend to be specific for a given pair of octahedral cations (Madejová *et al*., 1994; Bishop *et al*., 1999). This enables the vibrational components contributing to the peaks to be identified (Figure 1a) and, ultimately their quantitative contributions to the spectra to be determined (Figure 1b). Figure 1c shows that for a group of samples (nos. 7, 9–14) the NIR band areas (2(AlAlOH) + AlFeOH) diverged significantly from the general trend of increased octahedral Al occupancy with increasing band area. For this group of nontronites the octahedral Al occupancies, as assigned from conventionally calculated structural formulae (Table 2), were lower than the octahedral Al occupancies expected from NIR measurements (Figure 1c).

The use of NIR to determine octahedral Al contents of ferruginous smectites and nontronites is demonstrated in the case of Holland's Quarry (HQ-Tas, No. 12) nontronite. A conventional calculation of the structural formula of sample 12 would place nearly all of its available Al in tetrahedral sites (Table 2), but the NIR band area indicates that a substantial amount of Al exists in octahedral sites (Figure 1c). On fitting the integrated NIR band area to the curve for this nontronite, we estimate that 45% of its total Al (or 0.51 Al atoms per unit-cell) resides in octahedral sites (Figure 1c). Thus for this sample, NIR analysis predicts that ~11% of its total Fe^{3+} (0.42 Fe^{3+} atoms per unit-cell) occupies tetrahedral sites. Likewise (Table 3): Bingham (7) nontronite is estimated to contain ~3.5% of total Fe^{3+} (0.13 Fe^{3+} atoms); Mountainville (9) 2.5% (0.09 atoms); NG-1 (10) 17% (0.68 atoms); NAu-2 (11) 6% (0.24 atoms); HQ-Tas (12) 11% (0.42 atoms); Spokane (13) 10% (0.74 atoms); and CZ-Ger (14) 20% of total Fe^{3+} (0.91 Fe^{3+} atoms) in tetrahedral sites.

The polynomial regression that best predicts octahedral Al (Figure 1c) indicates that the results are accurate to ± 1.5% of total Fe^{3+} for those samples low in total Al (< ~6% Al_2O_3) and high in total Fe^{3+} (> ~36% Fe_2O_3). However, as the regression of the data in Figure 1a assumes that no Fe^{3+} is tetrahedrally coordinated in samples 1–6 and 8, the method fails to predict tetrahedral Fe^{3+} in most nontronites with < ~37% Fe_2O_3 (<3.6 Fe^{3+} atoms per unit-cell). This assumption means that tetrahedral Fe^{3+} may be undetected in some nontronites (Table 3).

X-ray diffraction of non-oriented powders

For Spokane (13) nontronite, which contains an exceptionally small amount of Al (Table 1), the *hk* profile simulations are consistent with the non-siliceous tetra-

Table 4. Observed ($|F^{obs}_{002}|/|F^{obs}_{003}|$) and calculated ($|F^{calc}_{002}|/|F^{calc}_{003}|$) structure amplitude ratios for the 002 and 003 reflections of oriented, ethylene glycol-solvated, Ca^{2+}-saturated films of nontronites and ferruginous smectites. The calculated structure amplitude ratios are specific to the chemistry of each sample.

		$\|F^{calc}_{002}\|/\|F^{calc}_{003}\|$						
		Number of Fe^{3+} occupying non-siliceous tetrahedral sites						Deduced tetrahedral Fe^{3+}
Sample	$\|F^{obs}_{002}\|/\|F^{obs}_{003}\|$	0	0.2	0.3	0.4	0.5	Max†	occupancy
2. SWa-1	0.64	0.64				0.20		nil
3. Cheney	1.05	0.99						nil
4. Giralong	1.31	1.59	1.05		0.72			0.10
5. Manito	1.40	2.32	1.48		1.01			0.23
6. NAu-1	1.42	2.43	1.66	1.26		0.62		0.26
7. Bingham	1.11	2.36	1.58		1.07			0.35
8. Garfield	1.32	2.49	1.54	1.29	1.06			0.30
9. Mountainville	1.45	2.66	1.66	1.36	1.12			0.34
10. NG-1	0.98	2.69	1.85		1.27		0.85	0.52
11. NAu-2	1.31	2.70					1.09	0.39
12. HQ-Tasmania	1.18	3.11			1.26			0.41
13. Spokane	1.25	3.34*				1.62**	1.40	0.74
14. CZ-Germany	1.16					1.75**	1.05	0.92

† Max refers to the Fe^{3+} occupancy of the maximum number of non-siliceous tetrahedral sites based on chemical analysis.
* For Spokane (13), value under '0' column signifies all Si in tetrahedral sites.
** the values under the '0.5' column for Spokane and CZ-Germany (14) were calculated using 0.67 and 0.69 Fe^{3+} atoms, respectively, as in their conventional structural formulae (Table 2)

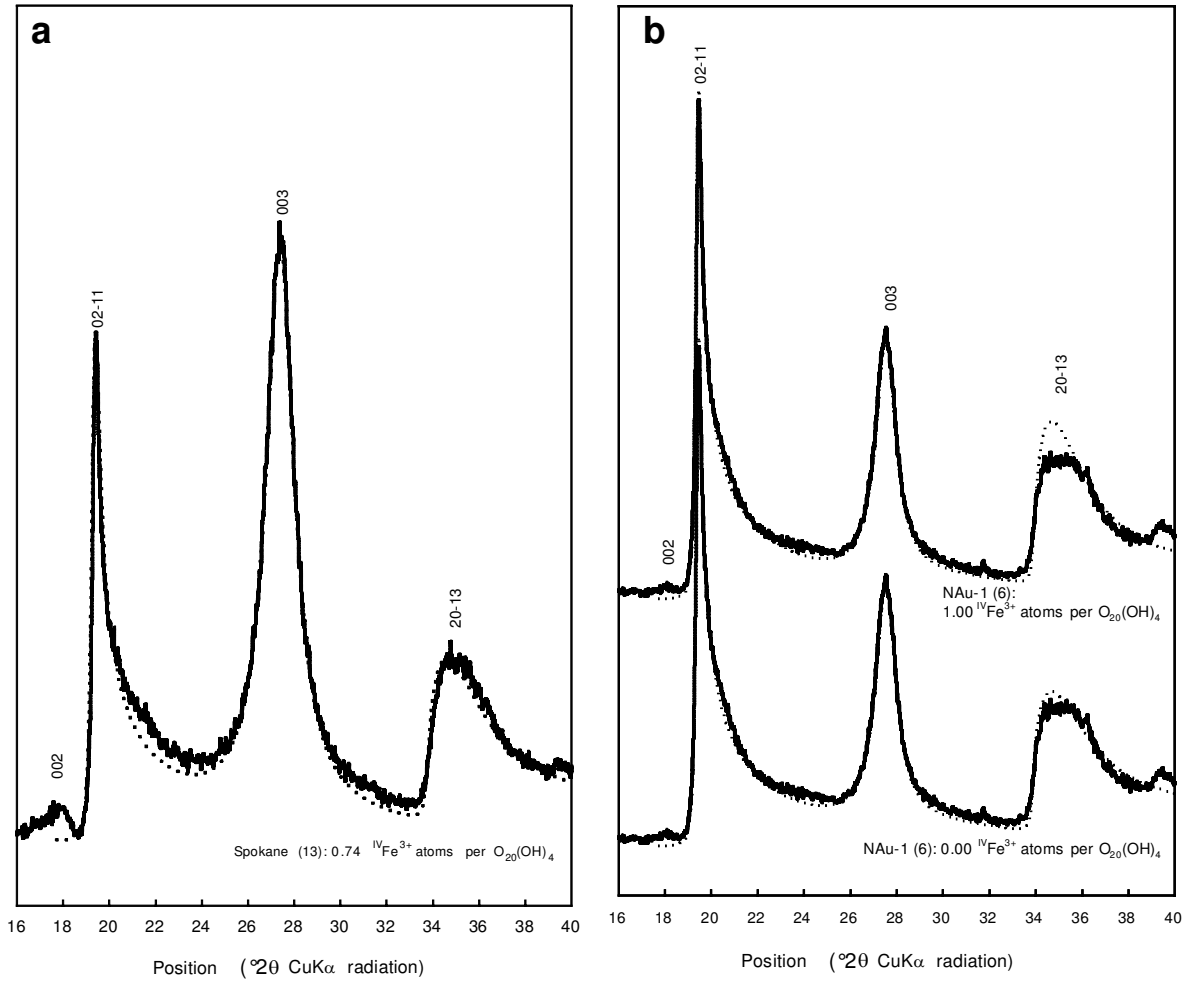

Figure 2. X-ray diffraction patterns of (a) Spokane nontronite (13) showing the fitted *hk* profile assuming Fe^{3+} occupies all (0.74) non-siliceous tetrahedral sites; (b) NAu-1 nontronite (6) assuming no tetrahedral Fe^{3+} (lower curve) or assuming Fe^{3+} occupies all (1.00) non-siliceous tetrahedral sites (upper profile); (c) (*facing page*) NAu-2 nontronite (11) assuming no tetrahedral Fe^{3+} (lower curve) or assuming Fe^{3+} occupies all (0.45) non-siliceous tetrahedral sites (upper profile).

hedral sites containing Fe^{3+} (Figure 2a). However, for NAu-1 (6) nontronite (Figure 2b), with its greater Al content, the best fit between the calculated and experimental *hk* profiles is obtained when tetrahedral Fe^{3+} is not present. The accuracy of this method is limited by the necessity of using completely dehydrated, random powder samples and of fitting the relative sizes of the disk-like coherent scattering domains (Manceau *et al.*, 2000). The sensitivity of the *hk* profile analysis depends on total Fe^{3+} content of a given sample, and is estimated to be ~50% of the non-siliceous tetrahedral sites in a given sample. The lack of sensitivity of the method is best illustrated in the case of NAu-2 nontronite (Figure 2c). Here, the fit with respect to both intensity and shape of the 02-11 and 20-13 reflections for no tetrahedral Fe^{3+} is nearly the same as when ~12% of total Fe^{3+} (0.45 Fe^{3+} atoms per unit-cell) is in the tetrahedral sites.

Despite the limitations described above, the results of fitting the *hk* profiles (Figure 2) are in good agreement with the results obtained by the other methods (Table 3). The result for Spokane (Figure 2a) agrees well with the value calculated from the chemical analysis (Table 2). By contrast, the results for SWa-1 (2), NAu-1 (6, Figure 2b) and Garfield (8) indicate that their tetrahedral sites do not contain Fe^{3+} (Table 3). For NG-1 (10) the results show that most, if not all, of the non-siliceous tetrahedral sites must be occupied by Fe^{3+} (Manceau *et al.*, 2000), in agreement with the other methods (Table 3). For NAu-2, as discussed above, the *hk* profile method shows little discrimination between the extreme cases of 0% or 12% of total Fe^{3+} in tetrahedral sites, and so the available non-siliceous tetrahedral sites may actually be occupied by Fe^{3+}.

X-ray diffraction of oriented films

Nontronite NG-1 (10), for example (Figure 3a), shows that the calculated ratio, $|F_{002}^{calc}|/|F_{003}^{calc}|$, decreases as the number of Fe^{3+} atoms in tetrahedral sites increases from

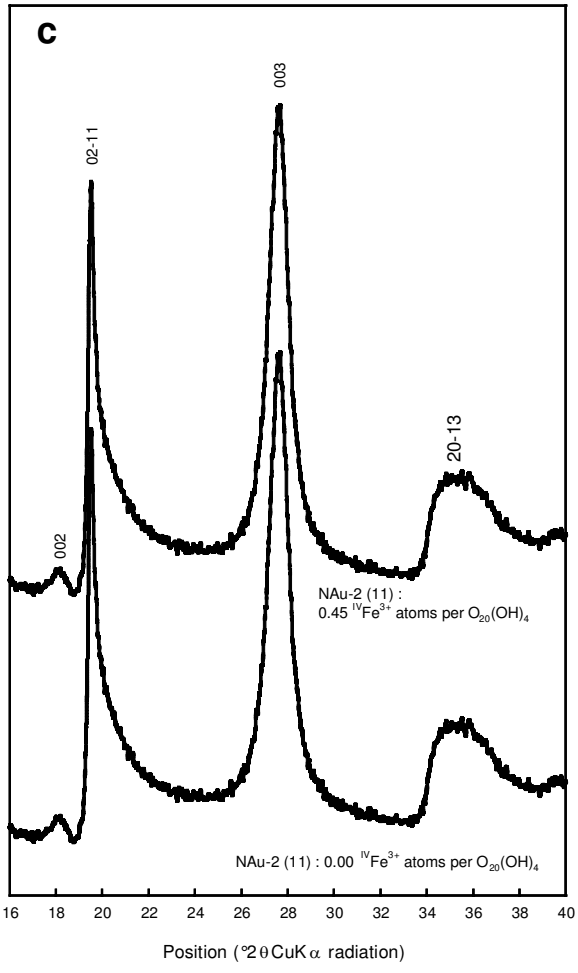

Figure 2(c).

0.0 to 0.8 (0–21% of total Fe^{3+}). Such changes for each sample allowed its tetrahedral Fe^{3+} site occupancy to be estimated by comparing its observed structure amplitude ratio with the ratios calculated for its specific chemistry and a range of site occupancies (Figure 3b and Table 4). Figure 3a and Table 4 show that for NG-1 the tetrahedral occupancy is 0.52 Fe^{3+} atoms per unit-cell (13.5% of total Fe^{3+}) and that the accuracy of the prediction is ~2–3% of total Fe^{3+} (0.1 Fe^{3+} atom per unit-cell). The detection limit for tetrahedral Fe^{3+} in nontronites by this method may be as low as ~3.0% of total Fe^{3+} (sample 5, Table 3). The accuracy and detection limit are dependent on the total Fe^{3+} content of the clay (Figure 3b) and, as can be seen from the shape of the curve in Figure 3a, also on the amount of Fe^{3+} in tetrahedral sites. The curve shown in Figure 3a is steeper at low tetrahedral Fe^{3+} occupancies, and this renders the technique particularly sensitive for these compositions.

The results from this technique predict that all the non-siliceous tetrahedral sites must be occupied by Fe^{3+} for the Spokane (13) and CZ-Ger (14) nontronites (Table 2), in which total Al is <1.7% Al_2O_3 (Table 1). Nontronites with compositions similar to Garfield (~36.5% Fe_2O_3; 7–8% Al_2O_3) may have as much as 4–12% their total Fe^{3+} in tetrahedral sites (Table 3).

X-ray pre-edge spectroscopy

X-ray pre-edge spectra of samples 2, 6, 8, 10, 11 and 13 (Figure 4a) show that intensity, position and shape differ from sample to sample. Enhancement of the Fe-K pre-edge intensity and the change in the pre-edge profile is attributed to increased structural disorder, due to a lowering of the local symmetry around 6-coordinated Fe^{3+} (Manceau and Gates, 1997) or to appreciable amounts of Mg and/or Al within octahedral sites (Manceau *et al.*, 2000). The error associated with estimations of tetrahedral Fe^{3+} occupancy from pre-edge spectra has been estimated to be as much as 10% of total Fe^{3+} (Manceau and Gates, 1997), depending on the sample. The detection limit for tetrahedral Fe^{3+} (Manceau *et al.*, 2000) is 3% of total Fe^{3+}. However, it should be noted that the reference samples used to estimate this value were $FePO_4$ and Garfield nontronite. Thus, Garfield nontronite was assumed to contain only octahedral Fe^{3+}. However, the results from the structure amplitude ratios, as well as earlier Mössbauer results (Bonnin *et al.*, 1985; Cardile and Johnston, 1985) indicate that Garfield may contain 7–8% of its total Fe^{3+} in tetrahedral sites. Thus, X-ray pre-edge spectroscopy may have underestimated the tetrahedral Fe^{3+} contents of the nontronites studied here.

A comparison of the spectra for Garfield (8), NAu-1 (6) and SWa-1 (2) indicates (Figure 4a) that the amplitude of the pre-edge peak increases as the total Al and/or total Mg content increases (Table 1). Thus, for SWa-1 and NAu-1, the enhanced pre-edge amplitude is probably due to distortion in the Fe^{3+} octahedra by mixing of Al and Mg within the octahedral sheet. However, for NG-1 (10), which contains similar Al and Mg contents to Garfield, the increased pre-edge amplitude cannot be related to distortions caused by these cations and supports instead, the presence of tetrahedral Fe^{3+} (Manceau *et al.*, 2000). Similarly for Spokane (13) and NAu-2 (11), which contain appreciably lower levels of Al, the increased amplitude of the pre-edge peak (Figure 4b) may result from tetrahedral Fe^{3+} being present in these samples.

Least-squares analysis (Figure 4b) shows that for Spokane (13) and NG-1 (10), ~10 and ~12%, respectively, of their total Fe^{3+} is tetrahedrally coordinated. The errors on these estimates are quite high and primarily due to our inability to model accurately the nontronite pre-edge spectral profile, especially on the higher-energy side. Despite this, we can estimate the error in the determination of tetrahedral Fe^{3+} to be ~5% of total Fe^{3+} (Figure 4b). Compared to the results from other methods (Table 3), this method estimates the amount of tetrahedral Fe^{3+} in Spokane to be 10% of total Fe^{3+} (or 0.46 atoms per unit-cell). This value is

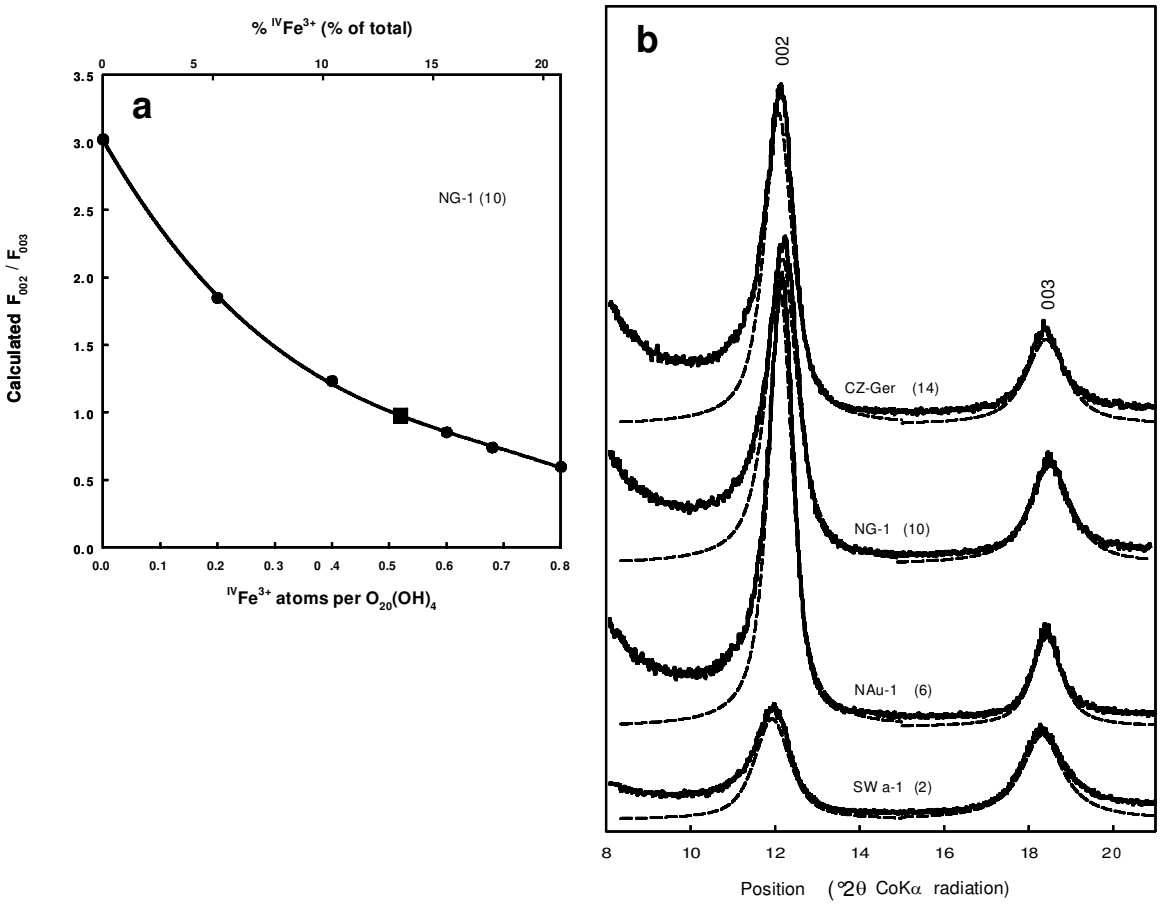

Figure 3. (a) Calibration of calculated structure amplitude ratios (solid circles) for NG-1 nontronite (10) as a function of tetrahedral Fe^{3+} content. The line represents the best fit on the calculated $|F_{002}|/|F_{003}|$ ratios used to estimate tetrahedral Fe^{3+} content from observed ratios. The solid square is the observed structure amplitude ratio measured on an orientated thin film of NG-1. Such a curve is required for each sample. (b) X-ray diffraction traces of oriented Ca^{2+}-saturated, ethylene glycol-solvated samples showing fitted 002 and 003 reflections used to obtain observed $|F_{002}|/|F_{003}|$ ratios.

unrealistically low, as there is insufficient Al in the sample to occupy the remaining non-siliceous tetrahedral sites. For NAu-2 (11), a best fit requires 8% of its total Fe^{3+} to be tetrahedrally coordinated (Table 3). While the pre-edge amplitude for this sample is enhanced relative to Garfield, it still retains the wider splitting between t_{2g}- and e_g-like energy states (Figure 4b). These pre-edge spectral characteristics could be consistent with a lowered symmetry about 6-coordinated Fe^{3+} (Manceau and Gates, 1997), rather than the presence of tetrahedral Fe^{3+}. In general, and relative to the other spectroscopies, the X-ray pre-edge spectroscopic method under-estimated the tetrahedral Fe^{3+} occupancy in nontronites. This is in contrast to previous studies on Fe oxyhydroxides (see for example, Manceau and Gates, 1997).

EXAFS

Figure 5a shows the K^3-weighted EXAFS spectra obtained after normalization for the amount of Fe^{3+} in the samples. Since the Fe-Fe and Fe-Al electronic waves are out of phase (Manceau *et al.*, 2000), the amplitude of normalized EXAFS spectra decreases with either increasing tetrahedral Fe^{3+} content or with increasing Al contents in the octahedra. Thus, the higher Al content of SWa-1 (a ferruginous smectite), rather than tetrahedral Fe^{3+}, is responsible for the lower amplitude of its spectra (Figure 5a). For NAu-1 (6) and Garfield (8), the spectra are similar, with only small amplitude differences in their 4 to 7 $Å^{-1}$ regions. These similarities follow from their similar compositions (Table 1). The amplitude of the spectra for the NG-1 (10), Spokane (13) and NAu-2 (11) nontronites are lower than that for Garfield, despite their lower Al_2O_3 contents. This reduction of the EXAFS signal is attributed to the presence of tetrahedral Fe^{3+} in these samples (Manceau *et al.*, 2000).

The RSFs (Figure 5b) also depend on structural details. The amplitude of peak A (Fe^{3+}–O interactions) depends on the number of oxygens surrounding Fe^{3+}, on

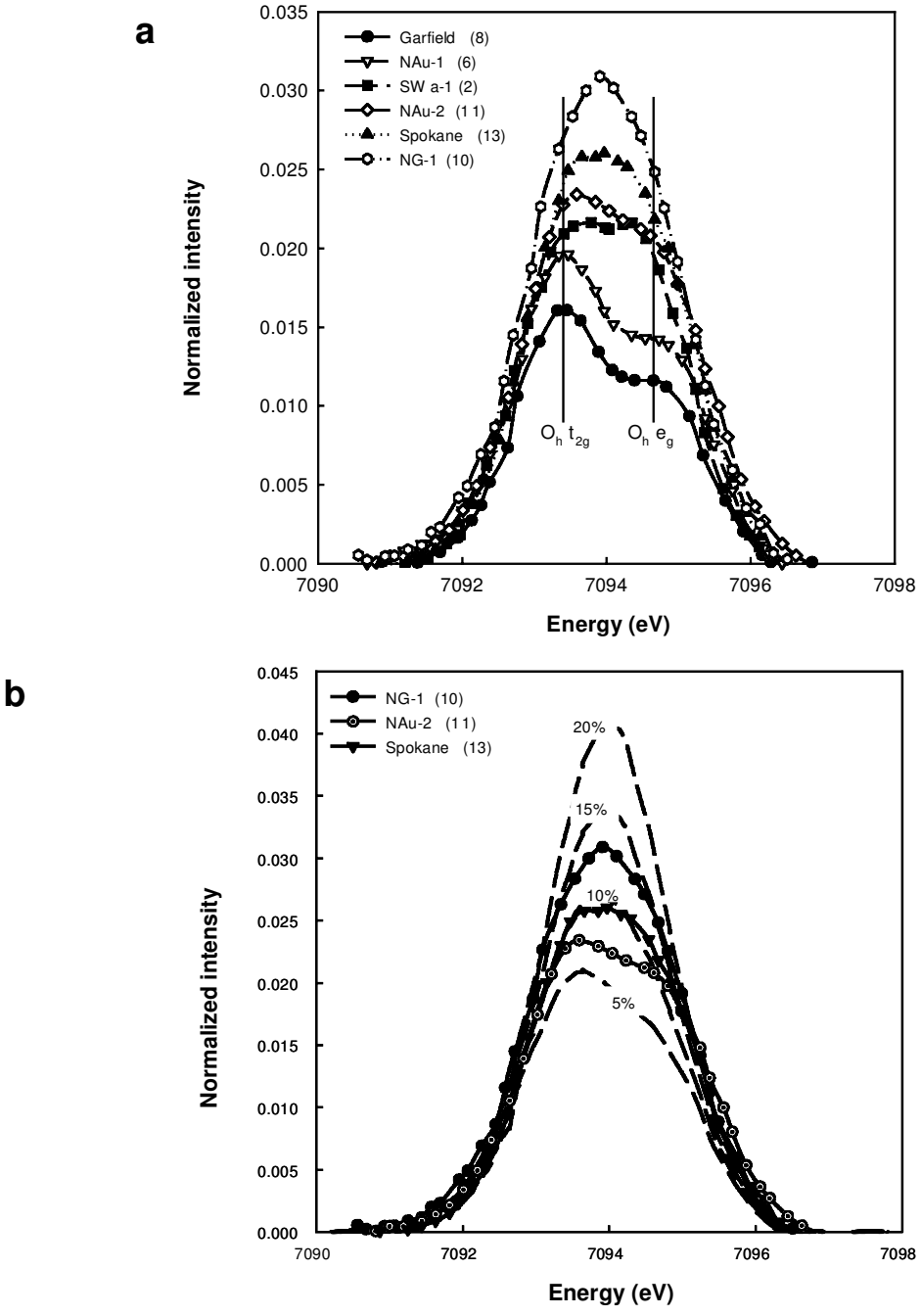

Figure 4. Normalized experimental Fe-K-pre-edge spectra of (a) selected nontronites and ferruginous smectite. (b) Calculated pre-edge spectra containing different tetrahedral Fe^{3+} contents used to estimate, by least-squares fitting, the tetrahedral Fe^{3+} composition for NG-1, NAu-2 and Spokane nontronites from their experimental pre-edge spectra.

the average Fe^{3+}–O bond distance and on the distribution of those distances. Thus, in comparison with Garfield (8), the decrease in amplitude of peak A (Figure 5b) for NG-1 (10), Spokane (13) and NAu-2 (11) is consistent with the tetrahedral Fe^{3+} being in these samples. In contrast for SWa-1, the decrease in amplitude of peak A (Figure 5b), is related to the increased spread in the Fe^{3+}–O bond distances due to this sample's greater Al and Mg^{2+} content (Manceau *et al.*, 2000). The shift of peak A to lower $R+\Delta R$ for Spokane is also consistent with an increased proportion of tetrahedral Fe^{3+}–O bonds, resulting in a lower overall average bond distance. For the NAu-2 sample, the position of peak A in Figure 5b is shifted slightly to larger Fe^{3+}–O bond distances, indicating that the environment about the octahedral Fe^{3+} is significantly

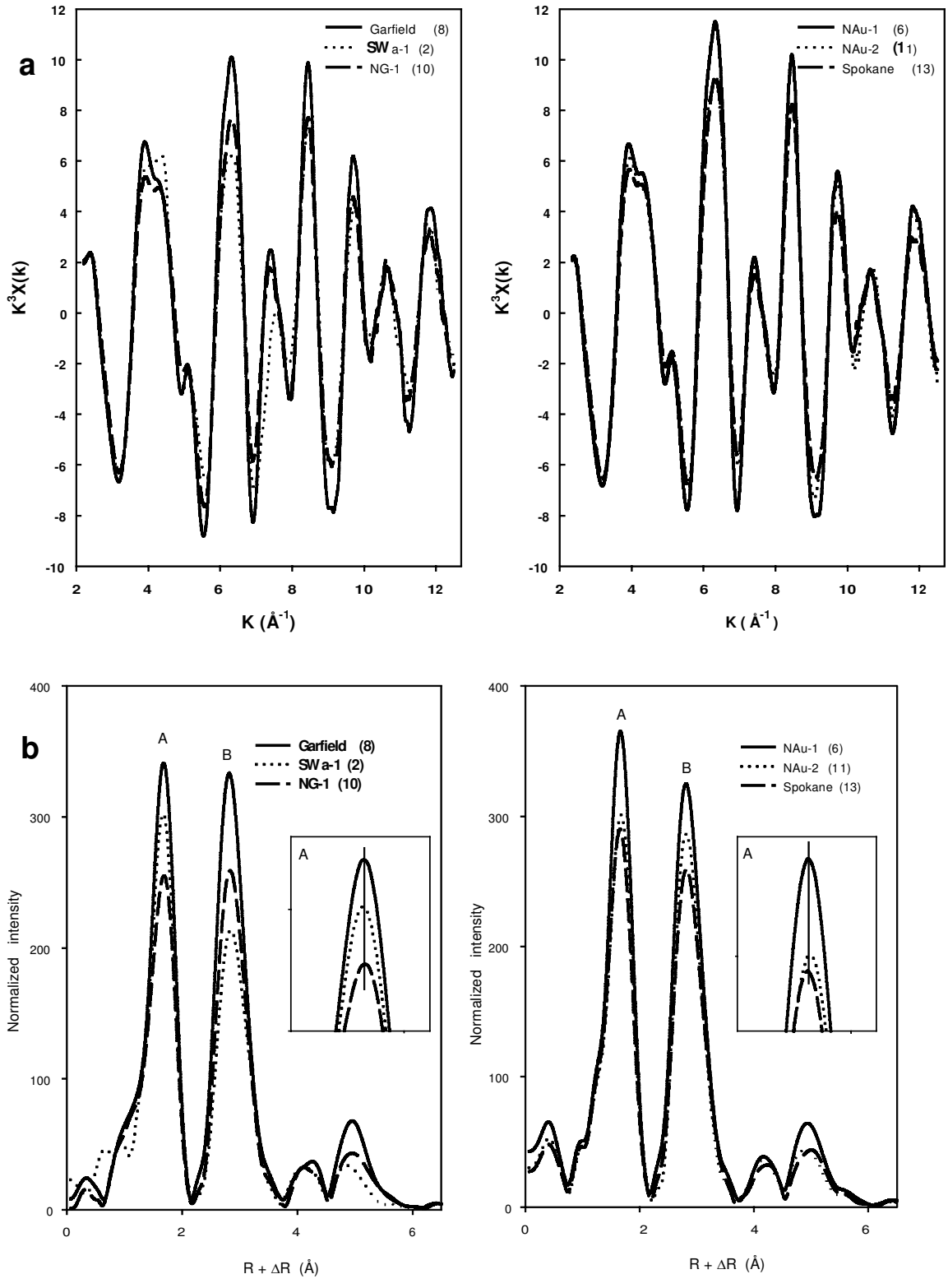

Figure 5. (a) Fe-k^3-weighted K-EXAFS spectra. (b) Radial structure functions, uncorrected for phase shift, of nontronites and ferruginous smectite. Insets: enlargements of peaks labeled A.

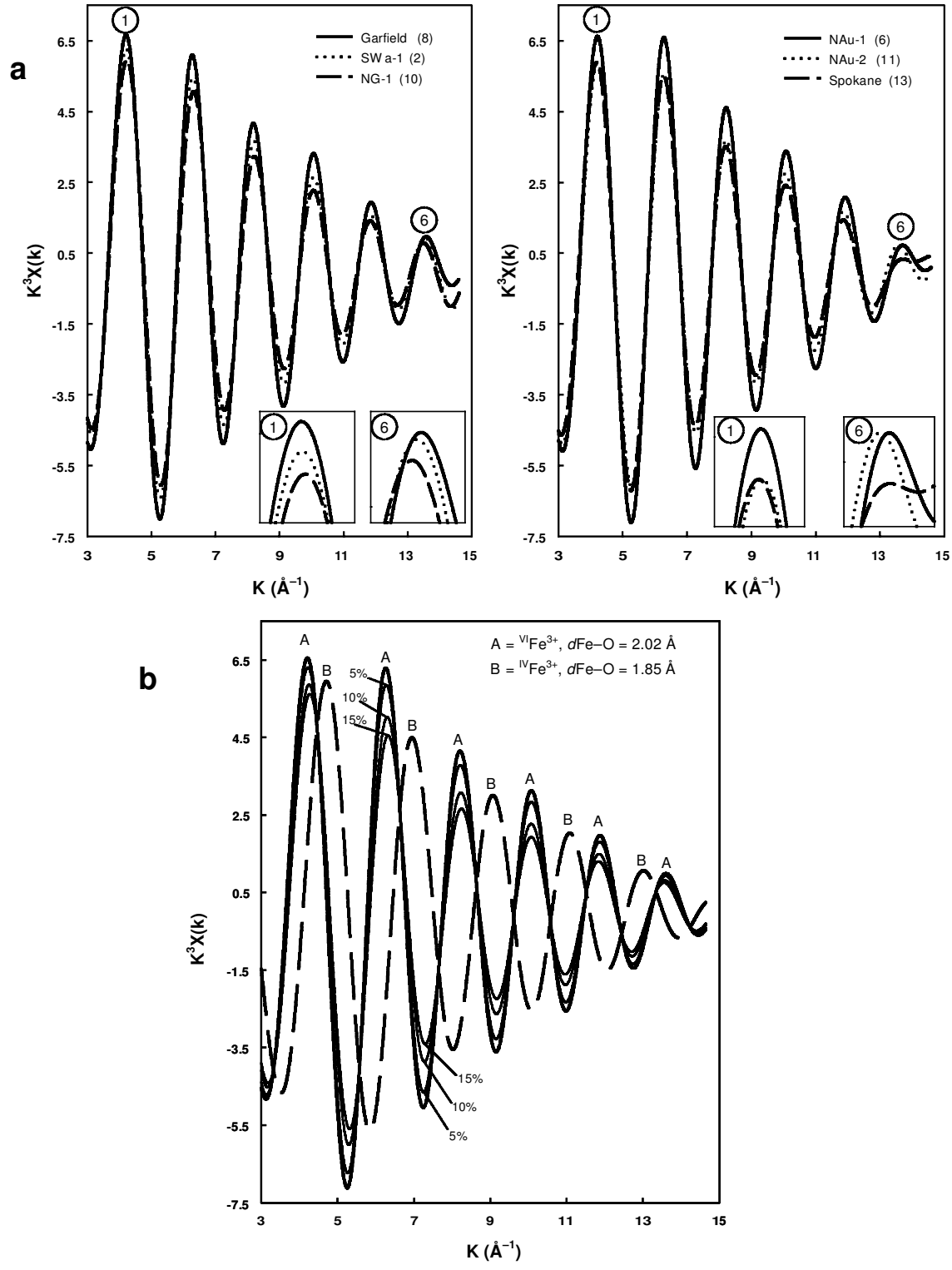

Figure 6. (a) Fourier back-transformation of peaks A in Figure 5b showing the Fe^{3+}–O contribution to the EXAFS spectra. Insets: enlargements of peaks 1 and 6. (b) Calculated Fe^{3+}–O contributions for octahedrally-coordinated Fe^{3+} with Fe^{3+}–O bond distance of 2.02 Å (waveform A), and tetrahedrally coordinated Fe^{3+} with Fe^{3+}–O bond distance of 1.85 Å (waveform B). Increasing percentages of tetrahedral Fe^{3+} causes both a loss of amplitude and a phase shift between the coordination/distance extremes.

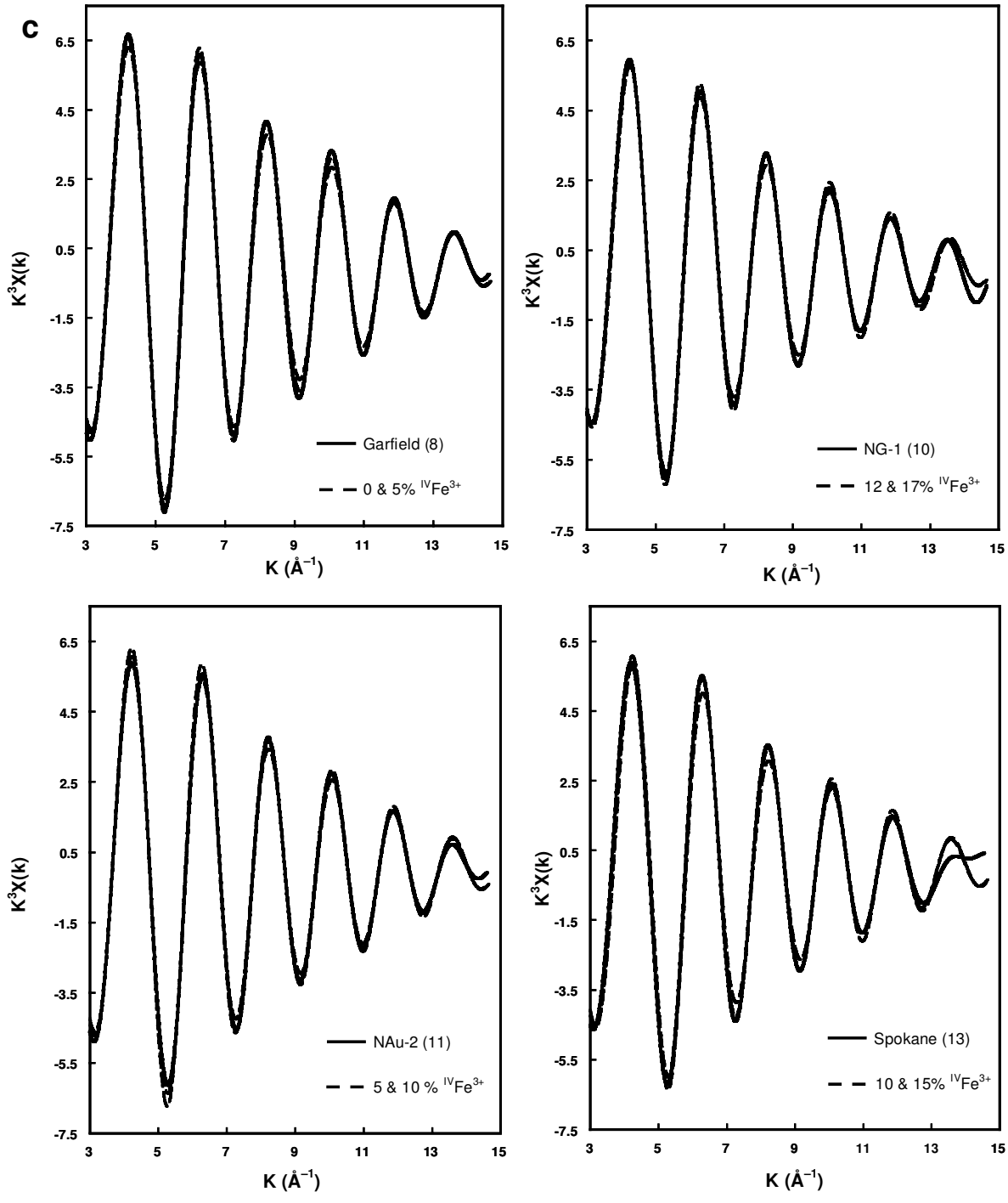

Figure 6(c). Least-squares fitting of the calculated Fe^{3+}–O waveforms (dashed lines) to estimate the tetrahedral Fe^{3+} composition for Garfield (8), NG-1 (10), NAu-2 (11) and Spokane (13) nontronites from their experimental waveforms (solid line).

distorted in this sample. The amplitude of peak B (composed of contributions from higher shells, *i.e.* nearest cations in octahedral and tetrahedral sites) is more difficult to interpret, but it depends on the chemical nature of the nearest cations, and on the spread of distances from those cations to the scattering center (Manceau *et al.*, 2000).

The experimental Fe^{3+}–O waveforms comprising peaks A in Figure 5b are shown in Figure 6a. The calculated k^3-weighted Fe^{3+}–O waveforms (Figure 6b)

for octahedrally coordinated Fe^{3+} (function A) have a greater amplitude and are shifted with respect to the Fe^{3+}–O waveforms corresponding to tetrahedrally coordinated Fe^{3+} (function B). On mixing in 5% tetrahedral Fe^{3+} (Figure 6b), a decrease in amplitude of the Fe^{3+}–O waveform occurs, but not a phase shift. After mixing ~15% tetrahedral Fe^{3+}, a phase shift can be discerned in addition to further reduction in the amplitude of the Fe^{3+}–O waveform. The experimental Fe^{3+}–O waveforms (Figure 6a) for NG-1 (10), NAu-2 (11) and Spokane (13) are all lower in amplitude and shifted in comparison to that for Garfield (8) and NAu-1 (6). Specifically, the waveforms for NG-1, Spokane and NAu-2, are right-shifted at low $Å^{-1}$ and left-shifted at high $Å^{-1}$ (Figure 6a) as in the simulations for 10–15% tetrahedral Fe^{3+} (Figure 6b). These phase shifts are consistent with shorter average Fe^{3+}–O bond distances and lower average coordinations for these samples (10, 11, 13). The Fe–O contributions for SWa-1 and NAu-1 are completely in phase with those for Garfield (Figure 6a).

Least-squares minimizations of experimental Fe–O waveforms indicate that ~15% of total Fe^{3+} (0.58 atoms per 22 oxygen equivalents) is in tetrahedral sites in NG-1, which agrees with the findings of Manceau *et al.* (2000), and ~12% (0.57 Fe^{3+} atoms) in Spokane (Figure 6c). As was the case for the X-ray pre-edge analysis, the tetrahedral Fe^{3+} occupancy estimated by this method for the Spokane nontronite is unrealistically low given its very low Al_2O_3 content. For NAu-2 (11), the best fit required that ~7% of its total Fe^{3+} be in tetrahedral sites. As a comparison, the amount of tetrahedral Fe^{3+} estimated for Garfield (8) by this method may be as high as ~3% of total Fe^{3+}. This value is near the detection limit of EXAFS, and the result is therefore inconclusive. Because cations other than Fe^{3+} can be present in tetrahedral and octahedral sites, the reference waveform chosen may not be completely suitable for a specific unknown sample.

Comparison between present and previous data

A sample by sample comparison of published data with the present data follows.

(1) For the ferruginous smectite SWa-1 (sample 2), Goodman *et al.* (1976) and Luca and Cardile (1989), using Mössbauer, estimated that 5% of the total Fe^{3+} is in tetrahedral sites. However, IR data presented by the first authors did not support this result, nor was the assignment of tetrahedral Fe^{3+} supported by the work of Lear and Stucki (1987) using Mössbauer, or by Manceau *et al.* (2000) using polarized-EXAFS. Luca and Cardile (1989) studied the <2 μm fraction of this material, which our XRD patterns show to contain goethite. For this reason we used the <0.2 μm fraction, which both Mössbauer spectroscopy and XRD showed to be pure. None of the methods described in the present work support the suggestion that there are significant amounts of tetrahedral Fe^{3+} in SWa-1, or in the other ferruginous smectites (*i.e.* samples 1–4).

(2) Published data exist for samples 5 and 8, representing nontronites with total Fe_2O_3 contents between 35.2 and 36.4%. However, Manito (API H33b) was mis-identified by Goodman *et al.* (1976) as Garfield (API H33a); see Kerr, (1951). Thus, the 9% tetrahedral Fe^{3+} reported was actually for Manito (sample 5), and not Garfield (sample 8). Cardile and Johnston (1985), using Mössbauer, also obtained 9%, and Lear and Stucki (1990) using magnetic susceptibility measurements, supported this result. Although the average value from the current study is ~3%, the upper threshold (8.5%) for the oriented film method (Table 3) agrees with published values.

(3) For Bingham (sample 7) nontronite Cardile and Johnston (1985) and Luca (1991), using Mössbauer spectroscopy, report 4 and 10% of total Fe^{3+}, respectively, being in tetrahedral sites. Our value of 6.5% tetrahedral Fe^{3+} (sample 7, Table 3), agrees with these published results.

(4) Garfield (sample 8) is the most widely studied nontronite and has caused considerable controversy. Rozenson and Heller-Kallai (1977), Besson *et al.* (1983), Bonnin *et al.* (1985), Johnston and Cardile (1985), Sherman and Vergo (1988), Lear and Stucki (1990), Murad *et al.* (1990), Luca (1991) and Manceau *et al.* (1998, 2000), among others, have attempted to determine its tetrahedral Fe^{3+} occupancy. Published values range from <1% (Bonnin *et al.*, 1985; Sherman and Vergo, 1988; Manceau *et al.*, 1998, 2000) to 13% (Luca, 1991) of total Fe^{3+}, with values estimated by the other authors falling between. For sample 8 the average of the present results is ~3%, but the upper threshold (10.5%) for the oriented powder method, and the estimate of 3% tetrahedral Fe^{3+} by EXAFS, are still within the range of published values.

(5) For the Höhen Hägen nontronite (NG-1, sample 10) the published values for tetrahedral Fe^{3+} are 10% (Komadel, 1990); 13–16% (Luca, 1991) and 17% (Manceau *et al.*, 2000). The value of 16.2% from the present work is within this range.

(6) For Spokane nontronite (sample 13), Johnston and Cardile (1985) report 7% and Luca (1991) between 3 and 6% tetrahedral Fe^{3+}. These results are too low, as Table 2 shows that this sample can have no less than 14.6% of its total Fe^{3+} in tetrahedral sites. From the current work, the average value of tetrahedral Fe^{3+} for Spokane is 15.3%.

(7) For Clausthal Zellerfeld nontronite (sample 14), Goodman *et al.* (1976) reported 15% tetrahedral Fe^{3+}. This is close to the average value of 19.8% from this work.

Recalculation of structural formulae

The data from Table 3 enable the structural formulae of nontronites to be recalculated as the average of the

Table 5. Structural formulae of nontronites following reassignment of Al and Fe^{3+} based on results given by the NIR, EXAFS and the two XRD methods as applied.

	1	2	3	4	5	6	7	8	9	10	11	12	13	14
Tetrahedral														
Si	7.58	7.40	7.06	7.32	7.07	6.98	7.17	7.02	7.01	7.12	7.55	6.98	7.26	7.04
Al	0.42	0.60	0.94	0.63	0.81	0.95	0.59	0.88	0.77	0.26	0.16	0.60	0.04	0.04
Fe				0.05	0.12	0.07	0.24	0.10	0.22	0.62	0.29	0.42	0.70	0.92
Σ	8.00	8.00	8.00	8.00	8.00	8.00	8.00	8.00	8.00	8.00	8.00	8.00	8.00	8.00
Octahedral														
Al	1.49	1.10	1.00	0.44	0.42	0.36	0.30	0.33	0.41	0.72	0.34	0.52	0.03	0.23
Fe	2.07	2.62	2.95	3.29	3.47	3.61	3.47	3.63	3.54	3.22	3.54	3.45	3.89	3.73
Mg	0.39	0.25	0.05	0.28	0.12	0.04	0.23	0.03	0.04	0.05	0.05	0.03	0.04	0.04
Σ	3.95	3.97	4.00	4.01	4.01	4.01	4.00	3.99	3.99	3.99	3.93	4.00	3.96	4.00
Total layer charge														
Tet	0.42	0.60	0.94	0.68	0.93	1.02	0.83	0.98	0.99	0.88	0.45	1.02	0.74	0.96
Oct	0.53	0.35	0.05	0.24	0.09	0.03	0.23	0.09	0.05	0.08	0.27	0.01	0.18	0.03
Σ	0.95	0.95	1.00	0.92	1.02	1.05	1.06	1.07	1.04	0.96	0.72	1.03	0.92	1.00

tetrahedral Fe^{3+} contents estimated from the various techniques (Table 5). However, in view of the uncertainties surrounding the results from the X-ray pre-edge absorption method, these were omitted from the recalculation. Following the reassignments of Al and Fe^{3+}, Table 5 shows that many nontronites do indeed contain more tetrahedral Fe^{3+} than indicated by their conventionally-calculated formulae (Table 2).

CONCLUSIONS

A combination of X-ray and NIR methods was used to determine how Fe^{3+} and Al are distributed over the available sites in a series of carefully-characterized, pure, homoionic nontronites and ferruginous smectites. The results show that nontronites may contain tetrahedral Fe^{3+} in substantial quantities when the Fe_2O_3 content is >37% (ignited basis). Eleven of the 12 nontronites studied contained more tetrahedral Fe^{3+} than required by conventional structural formulae calculations; four of these contained >10% of their total Fe^{3+} in tetrahedral sites. Of the remaining seven nontronites, three contain 5–10% of their total Fe^{3+} in tetrahedral sites, and the rest have < ~2–3% tetrahedral Fe^{3+}. The present results are comparable with published values.

The ease of application of the NIR method renders it a useful technique to determine Al and Fe^{3+} distributions, but analysis of structure amplitude ratios provides quantitative, *a priori* values when bulk chemistry of pure specimens is available. The other methods applied and discussed here (*e.g.* pre-edge, EXAFS) also provide useful information, but are not widely available. It should be stressed that spectroscopic methods can be limiting if they require comparisons to be made with reference materials that have assumed properties. Uncertainties in spectra decomposition can also limit their applicability.

ACKNOWLEDGMENTS

The authors would like to thank R.A. Eggleton, S. Hillier and I. Pontifex for providing some of the samples, J. Cashion for Mössbauer spectroscopy and P. Self for TEM analyses of the NAu-1 and NAu-2 nontronites. We also thank K. Norrish for insightful discussions on the chemistry of nontronites, J. Amonette, V. Luca and J. Madejová for constructive reviews, L. Janik for assistance with statistical analyses, M. Raven for assistance with X-ray powder diffraction and G. Rinder for drafting of figures.

REFERENCES

Besson, G., Bookin, A.S., Dainyak, L.G., Rautureau, M., Tsipursky, S.I., Tchoubar, C. and Drits, V.A. (1983) Use of diffraction and Mössbauer methods for the structural and crystallochemical characterisation of nontronites. *Journal of Applied Crystallography*, **16**, 374–383.

Besson, G., Drits, V.A., Dainyak, L.G. and Smoliar, B.B. (1987) Analysis of cation distribution in dioctahedral micaceous minerals on the basis of IR spectroscopy data. *Clay Minerals,* **22**, 465–478.

Bishop, J.L., Murad, E., Madejová, J., Komadel, P., Wagner, U. and Scheinost, A.C. (1999) Visible, Mössbauer and infrared spectroscopy of dioctahedral smectites: structural analysis of the Fe-bearing smectites Sampor, SWy-1 and SWa-1. Pp. 413–419 in: *Clays for Our Future. Proceedings 11th International Clay Conference, Ottawa, Canada* (H. Kodama, A.R. Mermut and J.K. Torrance, editors).

Bodine, M.W., Jr. (1987) CLAYFORM: A FORTRAN 77 computer program apportioning the constituents in the chemical analysis of a clay or other silicate mineral in a structural formula. *Computers and Geosciences,* **13**, 77–88.

Bonnin, D., Calas, G., Suquet, H. and Pexerat, H. (1985) Site occupancy of Fe^{3+} in Garfield nontronite: a spectroscopic study. *Physics and Chemistry of Minerals*, **12**, 55–64.

Busing, W.R., Martin, K.O. and Levy, H.A. (1962) ORFLS, a FORTRAN crystallographic least-squares refinement program. *Oak Ridge National Laboratory, Technical Manual* No. 305. 75 pp.

Cardile, C.M. and Johnston, J.H. (1985) Structural studies of nontronites with different iron contents by ^{57}Fe Mössbauer spectroscopy. *Clays and Clay Minerals*, **33**, 295–300.

Cardile, C.M. and Slade, P.G. (1988) Structural studies of

vermiculites with different iron contents by ^{57}Fe Mössbauer spectroscopy. *Neues Jahrbuch für Mineralogie Monatshefte,* 297–308.

Drits, V.A. and Tchoubar, C. (1990) *X-ray Diffraction by Disordered Lamellar Structures: Theory and Applications to Micro Divided Silicates and Carbons*. Springer Verlag, Berlin, 371 pp.

Dyar, M.D. (1987) A review of Mössbauer data on trioctahedral micas: evidence for tetrahedral Fe^{3+} and cation ordering. *American Mineralogist*, **72**, 102–112.

Dyar, M.D. (1993) Mössbauer spectroscopy of tetrahedral Fe^{3+} in trioctahedral micas – Discussion. *American Mineralogist,* **78**, 665–668.

Eggleton, R.A. (1977) Nontronite: chemistry and X-ray diffraction. *Clay Minerals*, **12**, 181–194.

Goodman, B.A., Russell, J.D., Fraser, A.R. and Woodhams, F.W.D. (1976) A Mössbauer and IR spectroscopic study of the structure of nontronite. *Clays and Clay Minerals*, **24**, 53–59.

Johnston, J.H. and Cardile, C.M. (1985) Iron sites in nontronite and the effect of interlayer cations from Mössbauer spectra. *Clays and Clay Minerals*, **33**, 21–30.

Keeling, J.L., Raven, M.D. and Gates, W.P. (2000) Geology and preliminary characterization of two nontronites from Uley graphite mine, South Australia. *Clays and Clay Minerals,* **46**, 537–548.

Kerr, P.F. (1951) *Preliminary report: Reference Clay Minerals. American Petroleum Institute. Research Project No. 49.* Columbia University, New York.

Klug, H.P. and Alexander, L.E. (1974) *X-ray Diffraction Procedures for Polycrystalline and Amorphous Materials.* Wiley-Interscience, New York, 966 pp.

Lear, P.R. and Stucki, J.W. (1987) Intervalence electron transfer and magnetic exchange in reduced nontronites. *Clays and Clay Minerals*, **35**, 373–378.

Lear, P.R. and Stucki, J.W. (1990) Magnetic properties and site occupancy of iron in nontronite. *Clay Minerals*, **25**, 3–13.

Luca, V. (1991) Detection of tetrahedral Fe^{3+} sites in nontronite and vermiculite by Mössbauer spectroscopy. *Clays and Clay Minerals*, **39**, 467–477.

Luca, V. and Cardile, C.M. (1989) Improved detection of tetrahedral Fe^{3+} in nontronite SWa-1 by Mössbauer spectroscopy. *Clay Minerals,* **24**, 555–559.

MacEwan, D.M.C. and Wilson, M.J. (1980) Interlayer and intercalation complexes of clay minerals. Pp. 197–248 in: *Crystal Structures of Clay Minerals and their X-ray Identification* (G.W Brindley and G. Brown, editors). Monograph, **5**, Mineralogical Society, London.

Madejová, J., Komadel, P. and Cecil, B. (1994) Infrared study of octahedral site populations in smecties. *Clay Minerals*, **29**, 319–326.

Manceau, A. and Gates, W.P. (1997) Surface structural model for ferrihydrite. *Clays and Clay Minerals*, **43**, 448–460.

Manceau, A., Bonnin, D., Stone, W.E.E. and Sanz, J. (1990) Distribution of Fe in the octahedral sheet of trioctahedral micas by polarized EXAFS. *Physics and Chemistry of Minerals*, **17**, 363–370.

Manceau, A., Chateigner, D. and Gates, W.P. (1998) Polarized EXAFS, distance-valence least-squares modeling (DLVS), and quantitative texture analysis approaches to the structural refinement of Garfield nontronite. *Physics and Chemistry of Minerals*, **25**, 347–365.

Manceau, A., Lanson, B., Drits, V.A., Chateigner, D., Gates, W.P., Wu, J., Huo, D. and Stucki, J.W (2000) Oxidation-reduction mechanism of iron in dioctahedral smectites: 1. Crystal chemistry of oxidized reference nontronites. *American Mineralogist*, **85**, 133–152.

Murad, E. (1987) Mössbauer spectra of nontronites: structural implications and characterization of associated iron oxides. *Zeitschrift für Pflanzenernahrung und Bodenkunde*, **150**, 279–285.

Murad, E., Cashion, J.D. and Brown, L.J. (1990) Magnetic ordering in Garfield nontronite under applied magnetic fields. *Clay Minerals*, **25**, 261–269

Norrish, K. and Hutton, J.T. (1969) An accurate X-ray spectrographic method for the analysis of a wide range of geological samples. *Geochimica et Cosmochimica Acta*, **33**, 431–453.

Plançon, A. (1981) Diffraction by layer structures containing different kinds of layers and stacking faults. *Journal of Applied Crystallography,* **14**, 300–304.

Rancourt, D.G. (1993) Mössbauer spectroscopy of tetrahedral Fe^{3+} in trioctahedral micas – Reply. *American Mineralogist* , **78**, 669–671.

Rancourt, D.G., Dang, M.-Z. and Lalonde, A.E. (1992) Mössbauer spectroscopy of tetrahedral Fe^{3+} in trioctahedral micas. *American Mineralogist*, **77**, 34–43.

Rémy, P. and Boullé, A. (1961) Sur le différentes variétés de phosphate de fer $FePO_3$ hydraté et anhydre. *Comptes Rendus de l'Academie des Sciences*, Paris, **253**, 2699–2701.

Rozenson, I. and Heller Kallai, L. (1977) Mössbauer spectra of dioctahedral smectites. *Clays and Clay Minerals*, **25**, 94–101.

Sakharov, B.A., Naumov, A.S. and Drits, V.A. (1982a) X-ray intensities scattered by layer structure with short range ordering parameters $S \geqslant 1$ and $G \geqslant 1$. *Doklady Akademii Nauk SSSR,* **265**, 871–874.

Sakharov, B.A., Naumov, A.S. and Drits, V.A. (1982b) X-ray diffraction by mixed-layer structures with random distribution of stacking faults. *Doklady Akademii Nauk SSSR,* **265**, 339–343.

Sherman, D.M. and Vergo, N. (1988) Optical (diffuse reflectance) and Mössbauer spectroscopic study of nontronite and related Fe-bearing smectites. *American Mineralogist* , **73**, 1346–1354.

Slade, P.G., Stone, P.A. and Radoslovich, E.W. (1985) Interlayer structures of the two-layer hydrates of Na- and Ca-vermiculites. *Clays and Clay Minerals*, **33**, 51–61.

Smoliar-Zviagina, B.B. (1993) Relationships between structural parameters and chemical composition of micas. *Clay Minerals,* **21**, 377–388.

(*Received 5 September 2000; revised 2 July 2001; Ms. 486; A.E. James E. Amonette*)